Published Quarterly
Mangalore, South India
ISSN 0972-5997
Volume 4, Issue 2; April-June 2005

Original Article

Chromosome Segmentation and Investigations using Generalized Gradient Vector Flow Active Contours

Authors

Albert Prabhu Britto, Research Scholar, Center for Medical Electronics, Dept. of ECE, Anna University, Chennai, 600 025, INDIA
Gurubatham Ravindran, Chairman, Faculty of Information and Communication Engineering, Anna University, Chennai, 600 025 INDIA

Address For Correspondence

A.Prabhu Britto, Research Scholar, Center for Medical Electronics, Dept. of ECE, Anna University, Chennai 600 025, INDIA
E-mail: britto_albert@ieee.org

Citation: Britto AP, Ravindran G. Chromosome Segmentation and Investigations using Generalized Gradient Vector Flow Active Contours *Online J Health Allied Scs.2005;2:3*

URL: http://www.ojhas.org/issue14/2005-2-3.htm

Open Access Archives

http://cogprints.ecs.soton.ac.uk/view/subjects/OJHAS.html
http://openmed.nic.in

Abstract:

We investigated Generalized Gradient Vector Flow Active Contours as a suitable boundary mapping technique for Chromosome spread images which have variability in shape and size, expecting to yield a robust segmentation scheme that can be used for segmentation of similar class of images based on optimal set of parameter values. It is found experimentally that a unique set of parameter values is required for boundary mapping each chromosome image. Characterization studies have established that each parameter has an optimal range of values within which good boundary mapping results can be obtained in similar class of images. Statistical testing validates the experimental results.

Key Words: Generalized Gradient Vector Flow, Active Contours, Deformable Curves, Chromosome, Boundary Mapping, Characterization

Introduction

Boundary Mapping is a segmentation approach that can be done easily in noise-free high contrast images employing low-level techniques, traditional edge detectors, region growing or mathematical morphology. These techniques are computationally fast. Noise and artifacts can possibly cause incorrect segmentation or boundary discontinuities in segmented objects.(1)

The classical boundary mapping techniques, namely, region growing, relaxation labeling, edge detection and linking use local information only. This leads to incorrect assumptions during the boundary integration leading to errors. Imaging conditions also introduce further variability in image characteristics.

A high-level segmentation technique, Active Contours, holds much promise for application to chromosome image segmentation. The main advantage of Active Contour models is the ability to generate closed parametric curves from images and the incorporation of a smoothness constraint that provides robustness to noise and spurious edges. The focus is on parametric deformable curves as they provide a compact, analytical description of object shape.

This work was conducted with an aim to use a parametric deformable curve formulation called Generalized Gradient Vector Flow (GGVF) field Active Contours to obtain accurate boundary mapping (segmentation) results from a class of chromosome images having variable shape, size and other variable image properties. The various parameters in the chosen active contour formulation were investigated for an optimal selection. The expected outcome would result in obtaining a universal set of parameter values that could be applied for successful boundary mapping a similar class of images.

Active Contour Models

Active Contours, also called as Snakes or Deformable Curves, first proposed by Kass et al.(2) are energy-minimizing contours that apply information about the boundaries as part of an optimization procedure. They are generally initialized around the object of interest by automatic or manual process. The contour then deforms itself from its initial position in conformity with the nearest dominant edge feature by minimizing the energy composed of the Internal and External forces. Internal forces which enforce smoothness of the curve are computed from within the Active Contour. External forces derived from the image help to drive the curve toward the desired features of interest during the course of the iterative process.

The energy function is minimized, thus making the model active. The energy minimization process can be viewed as a dynamic problem where the active contour model is governed by the laws of elasticity and lagrangian dynamics(3), and the model evolves until equilibrium of all forces is reached, which is equivalent to a minimum of the energy function.

Formulation of Active Contour Models

An Active Contour Model can be represented by a curve *C* as a function of its arc length τ,

$$c(\tau) = \begin{pmatrix} x(\tau) \\ y(\tau) \end{pmatrix}$$

-- (1) with τ=[0...1]. To define a closed curve c(0) is set to equal c(1). A discrete model can be expressed as an ordered set of n vertices

$\nu_i=(x_{i,}, y_i)^{\tau}$ with $\nu=(\nu 1,\ldots. \nu_n)$.

The large number of vertices required to achieve accuracy could lead to high computational complexity and numerical instability.(3)

Mathematically, an active contour model can be defined in discrete form as a curve $x(s)=[x(s),y(s),s\varepsilon$ [0,1] that moves through the spatial domain of an image to minimize the energy functional

$$E = \int_0^1 \frac{1}{2}(\alpha |x'(s)|^2 + \beta |x''(s)|^2) + E_{ext}(x(s))ds$$

-- (2) where α and β are weighting parameters that control the active contour's tension and rigidity respectively(4), and they govern the effect of the derivatives on the deformable curve. The first order derivative discourages stretching while the second order derivative discourages bending.

The external energy function E_{ext} is derived from the image so that it takes on its smaller values at the features of interest such as boundaries and guides the active contour towards the boundaries. The external energy is defined by

$$E_{ext} = \kappa | G\sigma(x,y) * I(x,y) | \quad -(3)$$

where $G\sigma(x,y)$ is a two-dimensional Gaussian function with standard deviation σ, $I(x,y)$ represents the image, and κ is the external force weight. This external energy is specified for a line drawing (black on white) and positive κ is used. A motivation for applying some Gaussian filtering to the underlying image is to reduce noise.

An active contour that minimizes E must satisfy the Euler Equation

$$\alpha x''(s) - \beta x''''(s) - \nabla E_{ext} = 0 \quad \text{-- (4) where}$$

$F_{int} = \alpha x''(s) - \beta x''''(s)$ and $F_{ext} = -\nabla E_{ext}$ comprise the components of a force balance equation such that $F_{int} + F_{ext} = 0$ –(5)

The internal force F_{int} discourages stretching and bending while the external potential force F_{ext} drives the active contour towards the desired image boundary. Eq. (4) is solved by making the active contour dynamic by treating x as a function of time t as well as s. Then the partial derivative of x with respect to t is then set equal to the left hand side of Eq. (4) as follows

$$x_t(s,t) = \alpha x''(s,t) - \beta x''''(s,t) - \nabla E_{ext} \quad \text{-- (6)}$$

A solution to Eq. (6) can be obtained by discretizing the equation and solving the discrete system iteratively.(2) When the solution $x(s,t)$ stabilizes, the term $x_t(s,t)$ vanishes and a solution of Eq. (4) is achieved.

Traditional active contour models suffer from a few drawbacks. Boundary concavities leave the contour split across the boundary. Capture range is also limited. Methods suggested to overcome these difficulties, namely multiresolution methods(5), pressure forces(6), distance potentials(7), control points(8), domain adaptivity(9), directional attractions(10) and solenoidal fields(11), introduced new difficulties.(12) Hence, a new class of external fields called Gradient Vector Flow fields(12,13) was suggested to overcome the difficulties in traditional active contour models.

Gradient Vector Flow (GVF) Active Contours

Gradient Vector Flow fields are obtained by solving a vector diffusion equation that diffuses the gradient vectors of a gray-level edge map computed from the image. These fields are used in Gradient Vector Flow (GVF) Active Contours. The GVF active contour model cannot be written as the negative gradient of a potential function. Hence it is directly specified from a dynamic force equation, instead of the standard energy minimization network.

The external forces arising out of GVF fields are non-conservative forces as they cannot be written as gradients of scalar potential functions. The usage of non-conservative forces as external forces enhance performance of Gradient Vector Flow field Active Contours compared to traditional energy-minimizing active contours.(12,13)

When the GVF field is very near to the boundary, it points towards the boundary,

but varies smoothly over homogeneous image regions extending to the image border. Hence the GVF field can capture an active contour from long range from either side of the object boundary and can force it into the object boundary. Information regarding whether the initial contour should expand or contract need not be given to the GVF active contour model.

The gradient vectors are normal to the boundary surface but by combining the Laplacian and the Gradient, the GVF field yields vectors that point into boundary concavities so that the active contour is driven through the concavities. Hence, the GVF active contour model is insensitive to the initialization of the contour, providing for flexible initialization and also able to move into boundary concavities. Also, the GVF is very useful when there are boundary gaps, because it preserves the perceptual edge property of active contours.(2,13)

The GVF field is defined as the equilibrium solution to the following vector diffusion equation(12),

$$u_t = g(|\nabla f|)\nabla^2 u - h(|\nabla f|)(u - \nabla f) \quad \text{-- (7a)}$$

$$u(x,0) = \nabla f(x) \quad \text{--- (7b)}$$

where, u_t denotes the partial derivative of $u(x,t)$ with respect to t, ∇^2 is the Laplacian operator (applied to each spatial component of u separately), and f is an edge map that has a higher value at the desired object boundary.

In Eq. (7a), $g(|\nabla f|)\nabla^2 u$ produces a smoothly varying vector field, and hence called as the "smoothing term", while $h(|\nabla f|)(u - \nabla f)$ encourages the vector field u to be close to ∇f computed from the image data and hence called as the data term. The weighting functions $g(\cdot)$ and $h(\cdot)$ apply to the smoothing and data terms respectively and they are chosen as $g(|\nabla f|) = \mu$ and $h(|\nabla f|) = |\nabla f|^2$.(13) $g(\cdot)$ is constant here, and smoothing occurs everywhere, while $h(\cdot)$ grows larger near strong edges and dominates at boundaries. The functions in "g" and "h" control the amount of diffusion in GVF.

Hence, the Gradient Vector Flow field is defined as the vector field

$V(x,y)=[u(x,y)v(x,y)]$ that minimizes the energy functional

$$\varepsilon = \iint \mu(u_x^2 + u_y^2 + v_y^2) + |\nabla f|^2 |v - \nabla f|^2 \, dxdy \quad \text{- (8)}$$

The effect of this variational formulation is that the result is made smooth when there is no data.

When the gradient of the edge map is large, it keeps the external field nearly equal to the gradient, but maintains the field to be gradually varying in homogeneous regions where the gradient of the edge map is small, i.e., the gradient of an edge map ∇f has vectors point toward the edges, which are normal to the edges at the edges, and have magnitudes only in the immediate vicinity of the edges, and in homogeneous regions ∇f is nearly zero.

μ is a regularization parameter that governs the tradeoff between the first and the second term in the integrand in Eq. (8).

The solution of Eq. (8) can be obtained using the Calculus of Variations. Further, u and v are treated as functions of time, and solved as generalized diffusion equations.(13)

Generalized Gradient Vector Flow (GGVF) Active Contours

In the GVF Active Contour formulation given by eq. (7), the term $g(\nabla f)$ is constant and hence smoothing occurs everywhere, while $h(\nabla f)$ grows larger near strong edges, dominating at boundaries. However when there are two edges in close proximity, it manifests as a long, thin indentation along the boundary. This makes the GVF tend to smooth between opposite edges. Hence the GVF loses forces to drive the Active Contour into this region.

Suitable weighting functions have been proposed in which $g(\cdot)$ becomes smaller as $h(\cdot)$ becomes larger.(14) Therefore there will be very little smoothing in the proximity of large gradients. Hence the effective vector field will be nearly equal to the gradient of

the edge map. There are many ways to specify these pairs of weighting functions, thus making the formulation a Generalized Gradient Vector Active Contour formulation.

From (14), the following weighting functions were chosen:

$$g(|\nabla f|) = e^{-\left(\frac{|\nabla f|}{\kappa}\right)^2}$$

--(9)

$$h(|\nabla f|) = 1 - g(|\nabla f|)$$ --(10)

This choice of weighting functions will make the computed GGVF field to conform to the edge map gradient at strong edges, but will vary smoothly away from boundaries. The solution remains the same as discussed previously under the subheading "GVF Active Contours".

Results and Discussion

The chromosome metaphase image (size 480 x 512 pixels at 72 pixels per inch resolution) was taken and preprocessed. Insignificant and unnecessary regions in the image were removed interactively. The chromosome of interest was user selected, by choosing a few points on the outer periphery of the chromosome of interest. These points formed the vertices of a polygon. Seed points for the initial contour were chosen by automatically selecting every third pixel on the perimeter of the polygon.

The GGVF deformable curve was allowed to deform until it converged to the chromosome boundary. The image was made to undergo minimal preprocessing so that the goal of boundary mapping in chromosome images with very weak edges is maintained. The GGVF Active contour is governed by the following parameters, namely, σ, μ, α, β and κ.

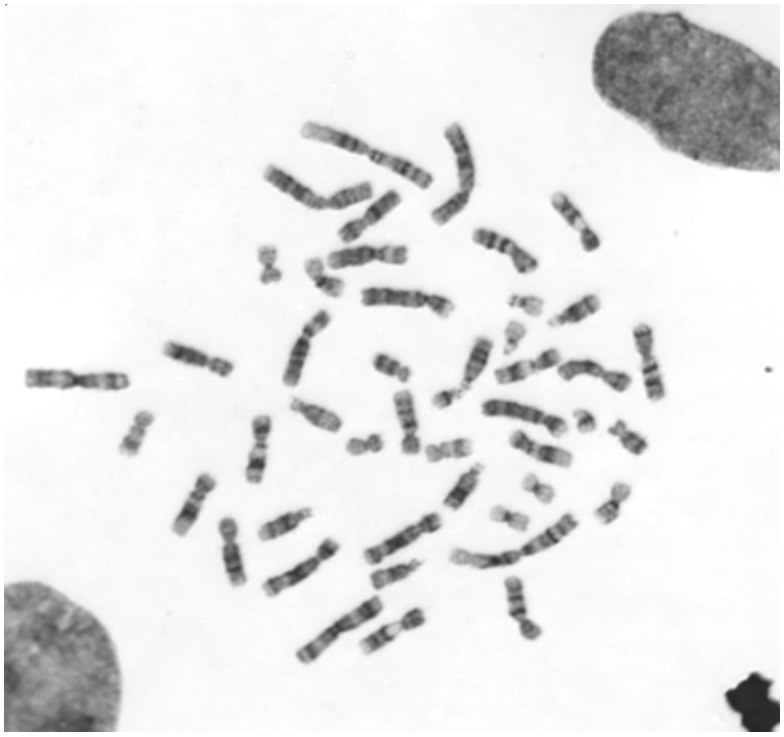

Chromosome Image

(Courtesy: Prof. Ken Castleman and Prof. Qiang Wu), Advanced Digital Imaging Research, Texas

σ determines the Gaussian filtering that is applied to the image to generate the external field. Larger value of s will cause the boundaries to become blurry and distorted, and can also cause a shift in the boundary location. However, large values of s are necessary to increase the capture range of the active contour. μ is a regularization parameter in Eq. (8), and requires a higher value in the presence of noise in the image.

α determines the tension of the active contour and β determines the rigidity of the contour. The tension keeps the active contour contracted and the rigidity keeps it smooth. α and β may also take on value zero implying that the influence of the respective tension and rigidity terms in the diffusion equation is low.

κ is the external force weight that determines the strength of the external field that is applied. The iterations were set suitably.

Characterization of each parameter was done and optimal parameter values were determined.

Experimental Results


Fig.1a Sample 1


Fig.2a Sample 2


Fig.3a Sample 3


Fig.4a Sample 4


Fig.5a Sample 5

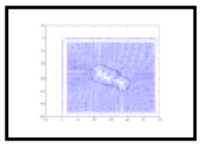
Fig.1b GGVF field 1

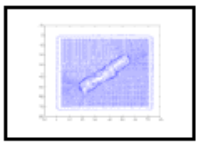
Fig.2b GGVF field 2

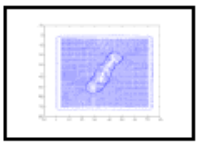
Fig.3b GGVF field 3

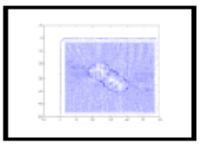
Fig.4b GGVF field 4

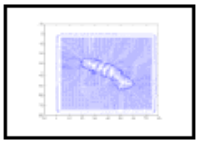
Fig.5b GGVF field 5


Fig.1c Output 1


Fig.2c Output 2


Fig.3c Output 3


Fig.4c Output 4


Fig.5c Output 5

The figures show original chromosome image samples, their corresponding GGVF fields and boundary mapped chromosome images. Fig. 1a shows original image sample, Fig. 1b shows its GGVF field, and Fig. 1c shows the output image, and hence forth for all five samples.

The graphical outputs show successful boundary mapping of chromosome images using GGVF Active Contours.

Experimental Validation

In order to quantify the performance of a segmentation method, validation experiments are necessary. Validation is typically performed using one or two different types of truth models. In this work, ground truth model is not available and hence validation is performed on ordinal or ranking scale and then quantified.

A set of 20 random samples is taken and characterization of each parameter is done. The outputs were tabulated in ranking order with "1" describing the best quality output and the rank increases up to rank "97" with decreasing quality. Rank "98" is a special case, where the output image is either rejected based on quality or the output image is not available due to numerical instability possibly caused due by the greater number of contour points.(3)

With other parameters taking on a constant value, each table represents characterization studies for each parameter denoting variation for only one parameter either between the lower and upper limits of the parameter or between the lower and upper limits that give significantly different output. Those parameter values where there is no significant difference between adjacent parameter values have not been tabulated. Also, those parameter values outside the tabulated range which gave no proper results have not been tabulated.

The parameter value that gives maximum good quality outputs for a majority of samples is chosen for characterization of the next parameter as follows. The statistical median is used to judge the distribution of values for each parameter value for all samples. When the median leans towards the lower values, i.e., towards "1", it indicates that almost 50% of the outputs lean towards "1" and hence that parameter value is chosen as the optimal one.

The characterization studies reveal that each parameter sometimes has an optimal range within which it can assume any value thereby giving majority good outputs for all samples. But for the sake of experimental purposes, only that investigated discrete value of each parameter that gave best output was chosen.

It is observed that there is very less variation among outputs given by closely separated parameter values and hence the variable increment is made high.

Sample	**Table1: Characterization of Sigma:** GGVF Sigma							
	0	0.25	0.5	0.75	1	2	3	4
Sample 1	77	77	77	77	13	13	35	39
Sample 2	77	13	13	13	13	13	13	33
Sample 3	77	78	77	77	29	9	35	37
Sample 4	79	77	77	77	29	15	15	39
Sample 5	97	97	97	97	97	97	97	97
Sample 6	97	97	97	97	97	97	97	97
Sample 7	97	97	97	97	97	97	97	97
Sample 8	86	86	86	86	86	45	50	42
Sample 9	78	78	78	78	13	13	15	29
Sample 10	77	77	77	77	77	13	29	29
Sample 11	79	78	78	78	29	29	29	46
Sample 12	97	97	97	97	97	97	97	97
Sample 13	97	97	97	97	97	97	97	97
Sample 14	97	77	86	77	77	37	38	45
Sample 15	97	77	77	77	29	77	75	29
Sample 16	79	77	77	77	29	29	29	29
Sample 17	80	78	78	78	13	32	40	48
Sample 18	77	77	77	13	13	29	77	31
Sample 19	79	77	77	77	77	29	29	31
Sample 20	78	86	86	86	46	50	36	46
Median	79	78	78	78	38	31	37	41

In Table 1, the median indicates that the acceptable optimal range of σ extends from 1 to 3. The best value compared qualitatively amongst those tested is 2 and hence it is chosen for performing further characterization.

Table 2: Characterization of Mu

Sample	GGVF Mu				
	0.005	0.01	0.05	0.1	1
Sample 1	13	13	35	97	97
Sample 2	13	13	11	97	97
Sample 3	11	9	39	97	97
Sample 4	15	15	29	97	97
Sample 5	97	97	97	97	97
Sample 6	97	97	97	97	97
Sample 7	97	97	97	97	97
Sample 8	86	45	45	97	97
Sample 9	31	31	31	97	97
Sample 10	29	29	57	97	97
Sample 11	29	29	45	97	97
Sample 12	97	97	97	97	97
Sample 13	97	97	97	97	97
Sample 14	70	37	44	97	97
Sample 15	77	77	57	97	97
Sample 16	13	29	45	97	97
Sample 17	31	32	48	97	97
Sample 18	11	29	11	97	97
Sample 19	29	29	77	62	97
Sample 20	38	50	50	97	97
Median	31	32	47	97	97

In Table 2, the median indicates that the acceptable optimal range of μ extends from 0.005 to 0.01. The best value compared qualitatively amongst those tested is 0.005 and hence it is chosen for performing further characterization.

Table 3: Characterization of Alpha

Sample	GGVF Alpha		
	0	0.5	1
Sample 1	13	45	93
Sample 2	13	13	13
Sample 3	11	97	59
Sample 4	15	31	97
Sample 5	97	58	97
Sample 6	97	86	97
Sample 7	97	97	97
Sample 8	86	94	97
Sample 9	31	31	97
Sample 10	29	29	77
Sample 11	29	45	97
Sample 12	97	97	97
Sample 13	97	97	97
Sample 14	70	97	97
Sample 15	77	49	57
Sample 16	13	45	97
Sample 17	31	48	97
Sample 18	11	50	97
Sample 19	29	45	97
Sample 20	38	57	61
Median	31	50	97

In Table 3, the median indicates that the acceptable optimal range of α extends from 0 to 0.5. The best value compared qualitatively amongst those tested is 0 and hence it is chosen for performing further characterization.

Table 4: Characterization of Beta

Sample	GGVF Beta		
	0	0.5	1
Sample 1	13	23	47
Sample 2	13	29	77
Sample 3	11	34	29
Sample 4	15	31	79
Sample 5	97	97	97
Sample 6	97	87	86
Sample 7	97	87	97
Sample 8	86	86	90
Sample 9	31	32	80
Sample 10	29	29	31
Sample 11	29	29	29
Sample 12	97	97	97
Sample 13	97	97	97
Sample 14	70	45	46
Sample 15	77	78	86
Sample 16	13	38	46
Sample 17	31	47	79
Sample 18	11	70	78
Sample 19	29	29	29
Sample 20	38	38	51
Median	31	42	79

In Table 4, the median indicates that the acceptable optimal range of ß extends from 0 to 0.5. The best value compared qualitatively amongst those tested is 0 and hence it is chosen for performing further characterization.

Table 5: Characterization of Kappa

Sample	GGVF Kappa						
	0.2	0.4	0.45	0.5	0.6	0.7	0.8
Sample 1	97	13	13	13	29	29	39
Sample 2	13	13	13	13	13	13	29
Sample 3	97	11	11	73	29	29	34
Sample 4	97	15	29	70	29	29	46
Sample 5	97	97	97	97	54	51	58
Sample 6	97	97	97	97	54	64	86
Sample 7	97	97	97	97	38	62	97
Sample 8	97	86	86	86	94	46	46
Sample 9	32	31	29	70	29	29	29
Sample 10	97	29	13	29	29	29	29
Sample 11	70	29	13	70	29	29	70
Sample 12	97	97	97	97	97	62	46
Sample 13	97	97	97	97	58	62	58
Sample 14	97	70	58	50	46	46	46
Sample 15	97	77	13	50	75	29	75
Sample 16	97	13	13	38	13	29	29
Sample 17	97	31	16	46	32	46	46
Sample 18	29	11	13	73	29	29	29
Sample 19	97	29	87	13	29	77	77
Sample 20	97	38	36	38	38	54	45
Median	97	31	29	70	31	38	46

In Table 5, the median indicates that the acceptable optimal range of κ extends from 0.4 to 0.7. The best value compared qualitatively amongst those tested is 0.45.

Hence the optimal set of parameter values that give good boundary mapping for the given class of chromosome images is σ = 2, μ = 0.005, α= 0, ß = 0 and κ= 0.45

A safe limit of 5% tolerance can be introduced to the optimal range of parameter values observed in each characterization.

Table 6: Optimal range of GGVF Active Contour parameter values for tested chromosome spread images

Parameter	Parameter Value used for tested spread image	Acceptable range of Parameter Values	Acceptable range of Values at 5% tolerance
GGVF Sigma	2	[1,3]	[0.9500, 3.1500]
GGVF Mu	0.005	[0.005, 0.01]	[0.0047, 0.0105]
GGVF Alpha	0	[0, 0.5]	[0, 0.5250]
GGVF Beta	0	[0, 0.5]	[0, 0.5250]
GGVF Kappa	0.45	[0.4, 0.7]	[0.3800, 0.7350]

This optimal range can be used for boundary mapping similar class of images.

Statistical Validation

The other parameters assume a constant value and their effect will also be felt on each characterization. In the course of the characterization study from Table 1 to Table 5, optimum values for the respective parameters are chosen and applied as constant in the successive table. In the last characterization study shown in Table 5, the values of σ, □□□□□and □ are assuming chosen optimal values and only κ is investigated, thereby yielding a one way variation. Hence, one way analysis of variance on Table 5 is sufficient to test the significance of the entire boundary mapping process, as a significant outcome from Table 5 justifies that the experimental results of Table 5 are valid, implying that the selected parameter values from Table 1 to Table 4 used as constants in Table 5 are also valid.

At the customary .05 significance level, one way Anova test yields a p value of 2.47728E-005 on Table 5, which rejects the null hypothesis. The very small p-value of 2.47728E-005 indicates that differences between the column means are highly significant. The test therefore strongly supports the alternate hypothesis that one or more of the samples are drawn from populations with different means. This implies that the results in Table 5 do not arise out of mere fluctuations, but the results are actually significant and that the experiment is valid. This justifies that a suitable value of parameter can be chosen from Table 5, and that the constant values of parameters and used in Table 5 are also valid. Therefore, the experimental results are significant and valid.

Validation Of Robustness Of The Scheme

The following difficulties were observed during the implementation of the boundary mapping scheme.

The banding pattern present in the chromosomes gives rise to higher contrast compared to the outer edges. This characteristic causes the GGVF external field to have a higher strength at the bands. Therefore, the GGVF Active Contour feels more attraction towards the bands than the outer boundary. Hence, the contour tends to cross the boundary into the inner regions seeking the bands.

The chromosome images in the chromosome spread image have variability in shape and size due to the nature of the spread image. Also, the spatial distribution of the chromosomes is random accompanied by uneven spacing between adjacent chromosomes. Hence, each chromosome in a chromosome spread image becomes a

unique sample demanding unique values of the parameters governing the GGVF Active Contour. There is also a need for unique number of iterations to converge.

The small object size of the chromosomes makes the computed GGVF field also to be small. Hence suitable choice of parameters is necessary; else the Active Contour crosses the boundary and results in a straight line at the axis of the chromosome sample.

The chromosomes in the spread image have a minor axis length varying between 14 and 17 pixels approximately and major axis length varying between 30 and 80 pixels approximately at 72 pixels per inch resolution. This causes the GGVF external field to have a high density at corners. Accompanied with the banding characteristic, the axis lengths force the GGVF Active Contour to map contours at the inner region of the chromosome instead of the actual boundary at the periphery of the chromosome.

The weak edges in chromosomes also contribute to the Active Contour to overwhelm weak edges and move into inner regions.

In addition to these inherent difficulties, more difficulty was introduced to validate the robustness of the boundary mapping scheme. The image was further degraded by transforming pixels having gray levels greater than 90% intensity in the range [0, 255]. This resulted in degradation of weak edges, giving rise to distorted edges and uneven boundary in the original image, offering more challenges to the task of segmentation using GGVF Active Contours.

These difficulties make the task of boundary mapping of chromosomes in chromosome spread images very difficult. Validations prove that the boundary mapping scheme has been very successful in spite of such difficulties. Hence the robustness of the scheme also stands validated.

Conclusion

The GGVF Active Contour establishes itself as a very good boundary mapping technique for chromosome spread images having chromosomes with variable shape, variable properties, and other variations introduced in imaging conditions.

Acknowledgments

The authors wish to thank Prof. Ken Castleman and Prof. Qiang Wu from Advanced Digital Imaging Research, Texas for their help in providing chromosome images.

References

1. McInerney T, Terzopoulos D. Deformable models in medical image analysis. IEEE Proceedings of the Workshop on Mathematical Methods in Biomedical Image Analysis. 1996. p171-180.

2. Kass M, Witkin A, Terzopoulos D. Snakes: active contour models. Int. J. Comp. Vision. 1987;1:321-331.

3. Rueckert D. Segmentation and tracking in cardiovascular MR images using geometrically deformable models and templates. PhD thesis. Imperial College of Science, Technology and Medicine. London. 1997.

4. Xu C, Prince JL. Gradient Vector Flow: A New External Force for Snakes. IEEE Proc. Conf. on Comp. Vis. Patt. Recog. (CVPR'97). 1997. p66-71

5. Leroy B, Herlin I, Cohen LD. Multi-resolution algorithms for active contour models. In 12th Intl. Conf. on Analysis and Optimization of Systems.1996:58-65.

6. Cohen LD. On active contours and balloons. CVGIP: Image Understanding. 1991 March;53(2):211-218.

7. Cohen LD, Cohen I. Finite-element methods for active contour models and balloons for 2-D and 3-D images. IEEE Trans. On Pattern Anal. Machine Intell. 1993 Nov.;15(11):1131-1147.

8. Davatzikos C Prince JL. An active contour model for mapping the cortex. IEEE Trans. on Medical Imaging. 1995 March;14(1):65-80.

9. Davatzikos C, Prince JL. Convexity analysis of active contour models. In Proc. Conf. on Info. Sci. and Sys. 1994. p581-587.

10. Abrantes AJ, Marques JS. A class of constrained clustering algorithms for object boundary extraction. IEEE Trans. on Image Processing. 1996 Nov.;5(11):1507-1521.

11. Prince JL, Xu C. A new external force model for snakes. In 1996 Image and Multidimensional Signal Processing Workshop. 1996. p30-31.

12. Xu C, Prince JL. Gradient Vector Flow Deformable Models. In Handbook of Medical Imaging. Academic Press. Sept. 2000.

13. Xu C, Prince JL. Snakes, shapes and gradient vector flow. IEEE Trans. on Image Processing. 1998 March;7(3):359-369.

14. Xu C, Prince JL. Generalized gradient vector flow external forces for active contours. Signal Processing. 1998;71:131-139.